International Journal of Control

ISSN: (Print) (Online) Journal homepage: https://www.tandfonline.com/loi/tcon20

Motion control of an articulated mobile manipulator in 3D using the Lyapunov-based control scheme

Avinesh Prasad, Bibhya Sharma, Jito Vanualailai & Sandeep Kumar

To cite this article: Avinesh Prasad, Bibhya Sharma, Jito Vanualailai & Sandeep Kumar (2021): Motion control of an articulated mobile manipulator in 3D using the Lyapunov-based control scheme, International Journal of Control, DOI: 10.1080/00207179.2021.1919927

To link to this article: https://doi.org/10.1080/00207179.2021.1919927

Published online: 30 Apr 2021.

INTERNATIONAL JOURNAL OF CONTROL
https://doi.org/10.1080/00207179.2021.1919927

Taylor & Francis
Taylor & Francis Group

Motion control of an articulated mobile manipulator in 3D using the Lyapunov-based control scheme

Avinesh Prasad, Bibhya Sharma, Jito Vanualailai and Sandeep Kumar

School of Computing, Information & Mathematical Sciences, The University of the South Pacific, Suva, Fiji

ABSTRACT

Finding feasible solutions to motion planning and control problem of robotic systems in different environments with various applications is an active area of research. This article presents a new solution to the motion planning and control problem of a three-dimensional articulated mobile manipulator comprising a car-like mobile platform and a three-dimensional *n*-link articulated arm using the Lyapunov-based control scheme. The motion of the system is described as twofold: first, the car-like mobile platform moves from an initial position to its pseudo-target, and second, when the mobile platform is within some predefined distance from the pseudo-target, the end-effector of the robot arm is attracted to its designated target. Therefore, presenting a new 2-Step Algorithm in this paper for dual movement of the articulated mobile manipulator in 3D. In addition, a workspace cluttered with fixed spherical and rod obstacles of random sizes and positions is considered in this research. For the mobile manipulator to avoid an obstacle, the Minimum Distance Technique is adapted where a point on the robot that is closest to an obstacle will avoid the obstacle. The convergence of the two bodies and the stability of the mechanical system are guaranteed by the Lyapunov's direct method. The continuous nonlinear control laws proposed from the control scheme also take into account all mechanical singularities and velocity limitations associated with the system. Theoretical proofs and computer simulations validate the new continuous, acceleration-based, nonlinear, time-invariant control laws.

ARTICLE HISTORY
Received 1 September 2020
Accepted 16 April 2021

KEYWORDS
Mobile manipulator; minimum distance technique; Lyapunov-based control scheme; navigation; total potentials

1. Introduction

There has been an escalating demand in recent years for robots to handle the dull, dirty, dangerous and difficult tasks which may be inaccessible or hazardous to humans (Cao et al., 2013; Chevalier et al., 2014; Sharma et al., 2015), mostly in highly unstructured or constrained environments and also outside the traditional factory settings (Hootsmans & Dubowsky, 1991). Amongst the other attributes of robots, high accuracy, cost and time efficiency, autonomy, reliability, independency, repeatability, and responsibility are ones seen highly desirable (Bunjaku et al., 2017; Mehta et al., 2017; Pajak & Pajak, 2017; Sharma et al., 2017).

Robotic mechanical systems such as aerial and ground vehicles, swimming and flying robots, parallel robots, car-like, tractor-trailer and mobile manipulators appear prominently in the literature and are commonly researched in different sectors for their inclusion in various real-world applications such as transportation, companionship, sampling, medical treatment and surgery, save and rescue, pursuit-evasion, surveying and explorations (Assaf et al., 2018; Bunjaku et al., 2017; Chevalier et al., 2014; Kumar et al., 2016, 2021; Matychyn, 2020; Mehta et al., 2017; Raj et al., 2020a; Sharma et al., 2015). Amongst all the existing and new robotic systems, the mobile manipulators have been emerged in the last decade as commercial tools which play an indispensable role to improve human livelihood and endeavours in health sectors and particularly in industries which require automation and repetition yet with high precision and accuracy (Bunjaku et al., 2017; Pajak & Pajak, 2017). The mobile manipulator is a robotic system built from manipulator(s) mounted on a mobile platform, noting that there is a broad spectrum of combinations possible; however, with a common viewpoint of optimising functionalities (mobility and dexterity) and reducing their limitations and restrictions (Hootsmans & Dubowsky, 1991; Pajak & Pajak, 2017). The mobile platform and the manipulator can be subjected to holonomic or nonholonomic constraints which give rise to four possible configurations of a mobile manipulator system (Sharma et al., 2012, 2017):

1. Type (h, h): both the platform and manipulator are holonomic.
2. Type (h, nh): the platform is holonomic while manipulator is nonholonomic.
3. Type (nh, h): the platform is nonholonomic while manipulator is holonomic.
4. Type (nh, nh): Both the platform and manipulator are nonholonomic.

In real-life applications, mobile manipulators can be of a great use for transportation, pick-and-place, and loading and unloading of objects from one mechanical system to another such as on to a trailer. As such, the mobile manipulator system

CONTACT Avinesh Prasad avinesh.prasad@usp.ac.fj

can be used for multiple purposes including the ones stated earlier. However, due to the coupled dynamics of the manipulator arm and the wheeled platform, the motion planning and control problem of the mobile manipulators is quite complex and computer intensive. In addition, the presence of holonomic and nonholonomic constraints in the system makes its kinematics complicated, nonlinear and underactuated (Papadopoulos & Poulakakis, 2000). Furthermore, the motion of the mobile manipulator is restricted because of the dynamic constraints associated with the system (Sharma et al., 2012, 2017). The limitations on steering angle, mechanical singularities of the links and the bounds on the velocities give rise to dynamic constraints which are difficult to integrate to the control design (Prasad et al., 2014; Sharma et al., 2012, 2017). It is also noted by researchers that if the workspace contains fixed or moving obstacles, the motion control problem becomes even more difficult and challenging. Researchers have enclosed the mobile platform and the links in smallest possible circles (Sharma et al., 2012, 2015, 2018b) which subsequently avoided the obstacles. A major drawback of this strategy is the high commitment of free space which may not allow the mobile manipulators to enter narrow passages or pass through close neighbouring obstacles. A better alternative has been the minimum distance technique designed by Sharma et al. (2017, 2018) which maximises the free space for optimal navigation.

The pioneering work on the motion control of mobile manipulators was carried out by Seraji (1998). Since then the motion planning and control of mobile manipulator systems have appeared frequently in the literature with significant research on problems such as trajectory planning (Sharma et al., 2012, 2015), configuration optimisation (Roennau et al., 2013), multi-tasking (Chen & Barnes, 2012; Sharma et al., 2017), formation control (Cui et al., 2010; Sharma et al., 2017; Shojaei, 2015), stability (Jaulin & Le Bars, 2013; Sharma et al., 2012, 2015), and obstacle avoidance (Khatib, 1986; Sharma et al., 2012; Yamamoto & Yun, 1995). These problems have been successfully with considered either single or multiple mobile manipulators, either with single or dual n-links, and either individual or cooperative tasks.

In the interest of brevity, we shall mention a few prominent ones only. Yamamoto and Yun (1995) presented a control method based on superquadric potential functions for coordinating mobile manipulators in the presence of obstacles. Tanner and Kyriakopoulos (2001) modelled a wheeled mobile manipulator system using Kane's dynamic equations. Papadopoulos et al. (2005) developed a polynomial-based approach for solving the obstacle avoidance problem of nonholonomic mobile manipulators. Boukattaya et al. (2011) proposed a robust adaptive control strategy for mobile manipulator system in the presence of parametric uncertainties and external disturbances. Other noteworthy contributions were made by Chung and Velinsky (1998) which deal with modelling and control of a mobile manipulator; Matsikis et al. (2003) proposed a behaviour coordination manager for a mobile manipulator; Padois et al. (2007) provided a unified modelling framework for the reactive control of wheeled mobile manipulators; Hamner et al. (2010) presented an autonomous mobile manipulator for assembly tasks; Djebrani et al. (2012) designed a nonlinear controller using the input-state linearisation method for controlling an omnidirectional mobile manipulator; and Buizza Avanzini et al. (2018) developed a controller based on constrained optimisation for tracking problems of mobile manipulators. Sharma et al. proposed a unique set of Lyapunov-based nonlinear controllers to control the motion of planar (Sharma et al., 2012), multiple (Sharma et al., 2015) and globally formation (Sharma et al., 2018) of n-link doubly nonholonomic manipulator(s).

In this paper, we have considered a holonomic manipulator arm mounted on a nonholonomic mobile platform, essentially a *Type* (nh, h) manipulator system. While the car-like mobile platform moves in a two-dimensional plane, the articulated arm can move in all directions, thus giving a three-dimensional motion of the entire system, and reaching the complete workspace. To solve the motion planning and control problem, a Lyapunov-based Control Scheme (LbCS) has been utilised that basically involves the construction of attractive and repulsive potential functions. These functions are summed appropriately as a Lyapunov function or total potentials – a basis to design the controllers of any robotic system (Khatib, 1986; Sharma et al., 2012, 2015, 2018b). This research work presents, for the first time in literature, a set of stabilising nonlinear, time-invariant, acceleration-based, continuous control laws using LbCS navigate a *Type* (nh, h) manipulator system, whilst obeying system constraints and singularities, and simultaneously avoiding obstacles in a three-dimensional bounded workspace. A novel two-step algorithm is designed which involves the convergence of the mobile platform to a pseudo-target and convergence of the end-effector to its designated target.

The main contributions of this paper are as follows:

1. *Motion of Mobile Manipulator in 3D Space*: While most of the work in the literature deal with motion and control in two-dimensional space due to the increased complexity of controllers and intensive computing, this paper deals in three-dimensional space within the ease in process.
2. *Control Laws*: A new set of stabilising and scalable nonlinear, time-invariant, acceleration-based, continuous control laws using LbCS navigate a *Type* (nh, h) manipulator system, whilst obeying system constraints and singularities, and simultaneously avoiding obstacles in 3D.
3. *Generalisation to n-links*: The mobile manipulator considered in this research has an n-link arm. We have therefore generalised the dynamic equations governing the motion of the mobile robot, the attractive and repulsive functions, the total potential function and the controllers to provide a collision free motion of the robot containing an arbitrary number of links.
4. *2-Step Algorithm*: The new algorithm ensures that the end-effector is not attracted to its target until the platform is at a certain distance from the pseudo-target. However, the arm has the freedom to move if it encounters obstacles during the entire journey of the mobile manipulator. The attraction potential functions also ensure that the total energy of the system remain continuous at all time.
5. *Obstacle Avoidance*: The Minimum Distance Technique (MDT) is utilised where the four sides of the mobile platform and each n-link avoid obstacles, thus maximising the free space. The scalable technique is, therefore,

better compared to Prasad et al. (2017); Raghuwaiya et al. (2016); Sharma et al. (2015) which involved enclosing the articulated bodies of the robots in smallest possible circles.

The reminder of the paper is organised as follows. The Lyapunov-based Control Scheme is detailed in Section 2 with an illustration of the total potentials. The dynamic model of the n-link mobile manipulator is derived in Section 3. In Section 4, the attractive potential functions are provided. The authors propose a new two-step algorithm in this section, where only the mobile platform is attracted to pseudo-target and when the centre of the platform is at a certain distance from the pseudo-target, then only the end-effector is attracted to its designated target. The obstacles avoidance scheme is discussed in Section 5. In particular, we have considered artificial obstacles arising from the dynamic constraints, fixed spherical and rod obstacles and the associated potential functions. The nonlinear acceleration-based continuous control laws are proposed in Section 6. Total potentials are designed from which the nonlinear control laws are extracted, and subsequently the stability issues pertaining to the robotic system are discussed. Computer simulation results are provided in Section 7 followed by conclusion and remarks on future work in Section 8.

2. Lyapunov-based control scheme

The governing principle behind the control scheme as proposed in Sharma et al. (2012, 2015) is to attach attractive field to the target and repulsive field to each obstacle. The main idea behind the control scheme is to design an appropriate Lyapunov function which acts as an energy function. The Lyapunov function is the sum of all attractive and repulsive potential functions. The repulsive potential functions are designed as ratios with the obstacle avoidance function in the denominator of each ratio and a positive *tuning parameter* in the numerator. The workspace is then inundated with positive and negative fields, with the direction of motion facilitated via the notion of steepest descent (Khatib, 1986; Sharma et al., 2012). For the robotic systems, the gradient of the total potentials determines the speed and the direction along which the robots move. The control laws are designed such that the Lyapunov function is decreasing for all $t \geq 0$ and vanishes to zero as $t \to \infty$.

As an illustration, consider a Lyapunov function of the form $L(x,y) = V(x,y)(1 + \sum_{l=1}^{3} \frac{\alpha_l}{W_l(x,y)})$ for some constants $\alpha_l > 0$. Here $V(x,y) > 0$ is an attractive potential function, while $W_l(x,y) > 0$ (for $l = 1, 2, 3$) are repulsive potential functions. Figure 1 shows the 3D visualisation of $L(x,y)$ and its contour plot.

3. The mobile manipulator model

Consider a three-dimensional mobile manipulator that has an articulated n-link arm with revolute joints fixed on a rotatable base mounted on a car-like mobile platform in the $z_1z_2z_3$-space as shown in Figure 2. The base can rotate through 360° along its principal axis via the revolute joint. The arm consists of multiple links made up of uniform slender rods; the first link can rotate through 180° with respect to the z_1z_2-plane while the other links can rotate through 180° with respect to the preceding link.

With reference to Figure 2, the following assumptions are made:

(i) the position of the centre of the car-like mobile platform is $(x_0, y_0, 0)$ and the orientation with respect to the z_1-axis is ϑ;
(ii) the three-dimensional robot arm is anchored on the point (x_0, y_0, a), where a is the sum of the height of the car plus the height of the rotatable base;
(iii) the ith link has a length of ℓ_i and angular position $\theta_i(t)$, measured from the z_1z_2-plane;
(iv) the base can rotate parallel to the z_1z_2-plane. The angular position of the base is $\theta_0(t)$, measured counterclockwise from the car's longitudinal axis;

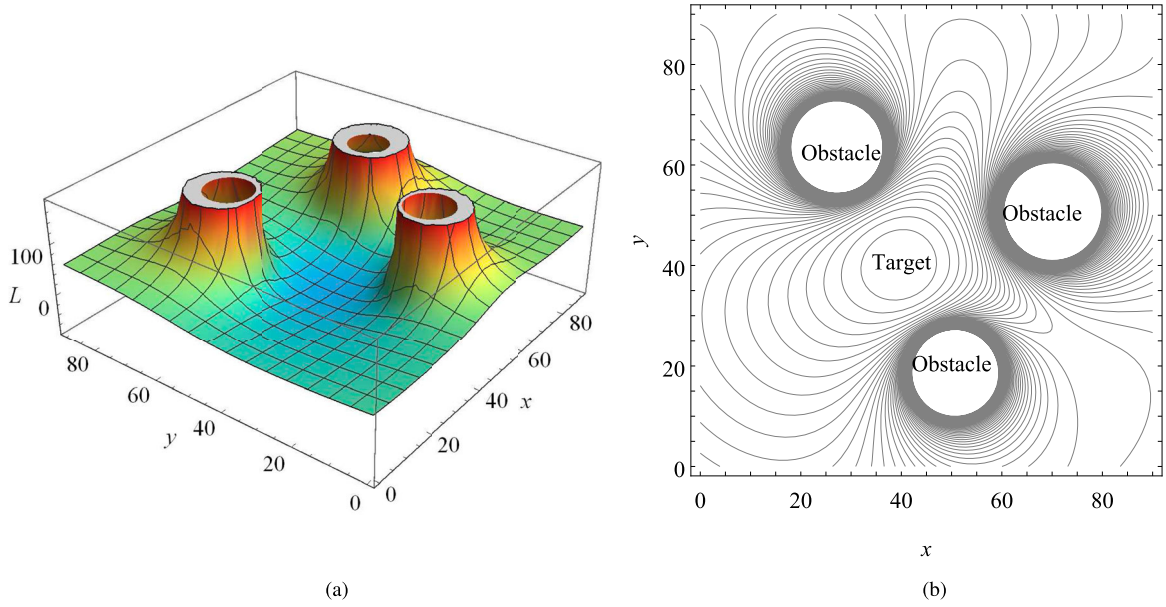

Figure 1. An illustration of Lyapunov function in 3D: (a) 3D visualisation of a Lyapunov function and (b) contour plot for the Lyapunov function.

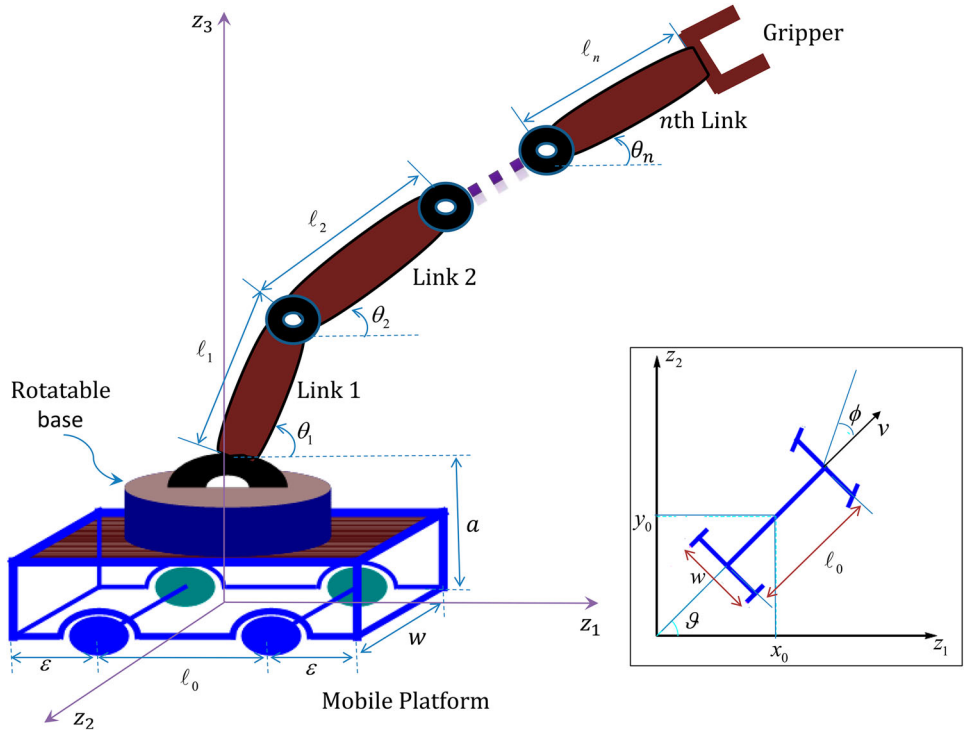

Figure 2. Schematic representation of a three-dimensional revolute manipulator mounted on a car-like mobile platform. Insert: The two-dimensional view of the mobile platform.

(v) the coordinate of the gripper (end-effector) is $(x, y, z) := (x_n, y_n, z_n)$.

Remark: It can be observed that the position of the end-effector of the mobile articulated manipulator arm can be expressed completely in terms of the state variables x_0, y_0, ϑ, and θ_i's as

$$\begin{aligned} x &= x_0 + \sum_{i=1}^{n} \ell_i \cos\theta_i \cos(\vartheta + \theta_0) \\ &:= x_{i-1} + \sum_{j=i}^{n} \ell_j \cos\theta_j \cos(\vartheta + \theta_0), \\ y &= y_0 + \sum_{i=1}^{n} \ell_i \cos\theta_i \sin(\vartheta + \theta_0) \\ &:= y_{i-1} + \sum_{j=i}^{n} \ell_j \cos\theta_j \sin(\vartheta + \theta_0), \\ z &= a + \sum_{i=1}^{n} \ell_i \sin\theta_i := z_{i-1} + \sum_{j=i}^{n} \ell_j \sin\theta_j. \end{aligned}$$

The rear wheel driven, steering angle control car-like vehicle model and the associated terminologies and notations are adopted from Sharma et al. (2015). Let ϕ denote the steering wheel's angle with respect to car's longitudinal axis, then the configuration of the car is given by $(x_0, y_0, \vartheta, \phi) \in \mathbb{R}^4$. For simplicity, it is assumed that $\dot{\vartheta} = \dot{\phi}$ (Sharma et al., 2012). Note that due to no slippage condition and no lateral movement, the velocities perpendicular to the two wheels are zero, which give rise to the platform's non-holonomic constraints (Sharma et al., 2012, 2015):

$$\begin{aligned} \dot{x}_r \sin\vartheta - \dot{y}_r \cos\vartheta &= 0, \\ \dot{x}_f \sin(\vartheta + \phi) - \dot{y}_f \cos(\vartheta + \phi) &= 0, \end{aligned}$$

where $(\dot{x}_f, \dot{y}_f)$ and $(\dot{x}_r, \dot{y}_r)$ are the velocities of front and rear wheels, respectively. Furthermore, if ℓ_0 is the distance between the two axles, ϵ is the safety parameter and w the length of each axle, then the kinematic model of the car-like vehicle is given by

$$\left.\begin{aligned} \dot{x}_0 &= v\cos\vartheta - \frac{\ell_0}{2}\varpi \sin\vartheta, \\ \dot{y}_0 &= v\sin\vartheta + \frac{\ell_0}{2}\varpi \cos\vartheta, \\ \dot{\vartheta} &= \frac{v}{\ell_0}\tan\phi := \varpi, \end{aligned}\right\} \tag{1}$$

where v and ϖ are the linear and angular velocities of the mobile platform, respectively. Suppose the angular velocity of the base and the ith link is ω_0 and ω_i, respectively, then the kinematic equations governing the motion of the n-link fully actuated manipulator are expressed as

$$\dot{\theta}_i(t) = \omega_i, \quad i = 0, 1, \ldots, n. \tag{2}$$

It is important to accommodate the dynamics of the system by including the acceleration components. The acceleration-based control laws will allow motion control at higher speeds (Sharma et al., 2012), whereas the kinematic models will reduce the significance of the results to low speeds. To obtain the dynamic model of the entire system, we combine system (1) and (2) and

add the acceleration components to get

$$\left.\begin{aligned}
\dot{x}_0 &= v\cos\vartheta - \frac{\ell_0}{2}\varpi\sin\vartheta,\\
\dot{y}_0 &= v\sin\vartheta + \frac{\ell_0}{2}\varpi\cos\vartheta,\\
\dot{\vartheta} &= \varpi, \quad \dot{\theta}_i(t) = \omega_i,\\
\dot{v} &= \rho_1 := \frac{F}{m}, \quad \dot{\varpi} = \rho_2 := \frac{\Gamma^*}{I^*}, \quad \dot{\omega}_i(t) = \sigma_i := \frac{\Gamma_i}{I_i},
\end{aligned}\right\} \tag{3}$$

where m is the mass of the car-like vehicle, F is the force along the car's longitudinal axis, Γ^* and Γ_0 are the torque about a vertical axis at (x_0, y_0), I^* is the moment of inertia of the car and I_0 is the moment of inertia of the base. Similarly, Γ_i and I_i, respectively, are the torque and moment of inertia of the ith link about the point $(x_{i-1}, y_{i-1}, z_{i-1})$. System (3) is a description of the instantaneous velocities and accelerations of the various components of the mobile manipulator. Here ρ_1, ρ_2 and σ_i, $i = 0, 1, 2, \ldots, n$ are classified as the nonlinear acceleration-based controllers. We shall use the vector notation $\mathbf{x} = (x_0, y_0, \vartheta, v, \varpi, \theta_0, \theta_1, \ldots, \theta_n, \omega_0, \omega_1, \ldots, \omega_n) \in \mathbb{R}^{2n+7}$ to refer to the positions and velocities of various components of the mobile robot arm. In particular, let $\mathbf{x}_0(t) = (x_0(t), y_0(t))$ and $\mathbf{x}_a(t) = (x(t), y(t), z(t))$, respectively, to refer to the rectangular positions of the mobile platform and the end-effector. Note that the steering angle ϕ is not part of the state–space variable in $\mathbf{x}$ due to our assumption that $\dot{\vartheta} = \dot{\phi}$. Moreover, the platform control variables are appropriately captured and expressed in the state variables which denote the control variables of the model and hence included in the Lyapunov-based Control Scheme.

4. Motion planning and control

Our main objective is to use the Lyapunov-based control scheme to derive the acceleration-based controllers (ρ_1, ρ_2 and σ_i) for the mobile manipulator. The main idea behind the control scheme is to design an appropriate Lyapunov function which acts as an energy function. We construct attractive and avoidance functions for the attraction to target(s) and repulsion from various obstacles, respectively. The Lyapunov function, also known as the total potentials, is the sum of all attractive and repulsive potential functions. We note that the repulsive potential functions are designed as ratios with the obstacle avoidance function in the denominator of each ratio and product of a positive *tuning parameter* and an auxiliary function in the numerator. We then design the control laws such that the Lyapunov function is decreasing for all $t \geq 0$ and vanishes to zero as $t \to \infty$.

We affix a target for the end-effector to reach after some time $t > 0$. The target is a sphere of centre (p_1, p_2, p_3) and radius r_T which is described as

$$T = \{(z_1, z_2, z_3) \in \mathbb{R}^3 : \|(z_1, z_2, z_3) - (p_1, p_2, p_3)\|^2 \leq r_T^2\}.$$

To ensure that the end-effector reaches its target without the manipulator fully stretching all the arms, it is necessary that $p_3 < a + \sum_{i=1}^{n} \ell_i$. Under this condition, for the end-effector to converge to its target, it is necessary that the mobile car-like platform should first converge to a pseudo-target which must lie in some neighbourhood of (p_1, p_2).

Definition 4.1: The set $\mathcal{N}$ described as

$$\mathcal{N} = \left\{(z_1, z_2) \in \mathbb{R}^2 : (z_1 - p_1)^2 + (z_2 - p_2)^2 \leq \left(\sum_{i=1}^{n} \ell_i\right)^2 - p_3^2\right\}.$$

is the neighbourhood of the point (p_1, p_2).

Let the centre of the pseudo-target be $(\tau_1, \tau_2) \in \mathcal{N}$ and radius R_T. We describe the pseudo-target as

$$T_0 = \{(z_1, z_2) \in \mathbb{R}^2 : (z_1 - \tau_1)^2 + (z_2 - \tau_2)^2 \leq R_T^2\}.$$

We will use the vector notation $\mathbf{e}_0 = (\tau_1, \tau_2)$ and $\mathbf{e}_a = (p_1, p_2, p_3)$ to refer to the positions of the pseudo-target and the target, respectively.

4.1 The two-step algorithm

In this research, a new algorithm known as the two-step algorithm is proposed to assist the LbCS in facilitating the motion planning and control problem of the mobile manipulator:

Step 1: The car-like mobile platform will move from the initial position, $\mathbf{x}_0(0)$ to the pseudo-target, $\mathbf{e}_0$. At this time, the end-effector is not attracted to its target until the centre of the mobile platform is within a distance of, say, $c > 0$ from the pseudo-target, i.e. when $(x_0 - \tau_1)^2 + (y_0 - \tau_2)^2 > c^2$. (However, the obstacle avoidance scheme will be active for both bodies.)

Step 2: When the mobile platform is within a user-defined distance of $c > 0$ from the pseudo-target, the end-effector will be attracted to its target centred at $\mathbf{e}_a$.

4.2 Pseudo-target and target attractions

For attractions to the pseudo-target and target, we consider the following attractive potential functions:

$$V_1(\mathbf{x}) = \frac{1}{2}\left[(x_0 - \tau_1)^2 + (y_0 - \tau_2)^2 + v^2 + \varpi^2\right], \tag{4a}$$

$$V_2(\mathbf{x}) = \frac{h_c}{2}\left[(x - p_1)^2 + (y - p_2)^2 + (z - p_3)^2\right] + \sum_{i=0}^{n} \omega_i^2, \tag{4b}$$

are designed for the attraction to the pseudo-target and target, respectively, where

$$h_c = \begin{cases} 0, & \text{if } (x_0 - \tau_1)^2 + (y_0 - \tau_2)^2 \geq c^2; \\ [c^2 - (x_0 - \tau_1)^2 - (y_0 - \tau_2)^2]^2, & \text{otherwise.} \end{cases}$$

The h_c function will ensure that the end-effector is not attracted to its target until the centre of the mobile platform is within a

distance of $c > 0$ from the pseudo-target. Due to the nature of the attractive potential functions, these functions are *continuous everywhere and have continuous first partial derivatives everywhere*, including the points that lie on the circle $(x_0 - \tau_1)^2 + (y_0 - \tau_2)^2 = c^2$. Hence the motion of the mobile robot will be continuous for all time $t \geq 0$.

4.3 Configuration of the Arm when $h_c = 0$

Looking at the form of $V_2(\mathbf{x})$, when $h_c = 0$ the arms are not attracted to the target, however, the arm's angular velocities have the freedom to change if any of its link comes near to an obstacle. Consequently, the links must re-achieve their initial configuration after avoiding the obstacle. For this, the potential function is given as

$$V_3(\mathbf{x}) = \frac{\kappa}{2}\left(1 - \frac{h_c}{c^2}\right)\sum_{i=0}^{n}(\theta_i - \theta_i(0))^2, \tag{5}$$

where $\kappa > 0$ is the angle gain. A larger value of κ would mean that the links re-achieve their initial configuration faster when compared to a smaller value of κ.

5. Avoidance of obstacles

In this section, possible forms of obstacles that can be encountered by the navigating mobile manipulator are considered. In particular, the research considers:

1. Artificial obstacles – These are the mechanical singularities associated with the system. In particular, this study considers the singular configuration of the arms and the limitations on the various velocities and the steering angle of the mobile platform (Sharma et al., 2012, 2015, 2017).
2. Fixed obstacles – The study considers stationary spherical and rod obstacles within the workspace that can possibly obstruct the motion of the mobile manipulator.

For effective obstacle avoidance, when any part of the robot comes near to an obstacle, the robot should appropriately reduce its speed and the various bodies must correctly deviate away from the obstacle.

5.1 Artificial obstacles

The steering and link angles of the robot are limited due to the mechanical singularities, while the velocities must be bounded for safety reasons (Raj et al., 2020b; Sharma et al., 2012, 2015, 2017). These restrictions are explained below:

1. Bound the linear velocity of the mobile platform as $|v(t)| \leq v_{\max}$, where $v_{\max} > 0$ is the maximum velocity of the car-like mobile platform.
2. Bound the velocities of the rotatable base and links as $|\omega_i(t)| \leq u_{\max}$ for $i = 0, 1, \ldots, n$, where $u_{\max} > 0$ is the maximum angular velocity of the rotatable base/link.
3. The steering angle of the car is restricted as $|\phi(t)| \leq \phi_{\max} < \frac{\pi}{2}$, where $\phi_{\max}$ is the maximum steering angle (Sharma et al., 2015). To satisfy this restriction, we impose the inequality $|\varpi| < \frac{v_{\max}|\tan(\phi_{\max})|}{\ell_0} := \varpi_{\max}$.
4. The motion of the end-effector is restricted in the sense that no two adjacent links can neither be fully stretched nor it can folded back (Sharma et al., 2012). That is, $0 < |\theta_i - \theta_{i-1}| < \pi$ for $i = 2, 3 \ldots, n$.
5. The motion of Link 1 is restricted as $0 < \theta_1 < \pi$.

For the restrictions on velocities, the following avoidance functions are constructed:

$$U_1(\mathbf{x}) = \frac{1}{2}(v_{\max}^2 - v^2), \tag{6a}$$

$$U_2(\mathbf{x}) = \frac{1}{2}\left(\frac{v_{\max}^2\tan^2(\phi_{\max})}{\ell_0^2} - \varpi^2\right), \tag{6b}$$

$$U_{3+i}(\mathbf{x}) = \frac{1}{2}(u_{\max}^2 - \omega_i^2) \tag{6c}$$

for $i = 0, 1, \ldots, n$. We will see later in Section 6 that each of these functions will be added as a ratio to form the repulsive potential field functions for the Lyapunov function of the system, as outlined in Section 2. Similarly, for restrictions on angles, the following avoidance functions are constructed:

$$S_1(\mathbf{x}) = \theta_1, \quad S_2(\mathbf{x}) = \pi - \theta_1, \tag{7a,b}$$

$$S_{i+1}(\mathbf{x}) = |\theta_i - \theta_{i-1}|, \quad S_{i+n}(\mathbf{x}) = \pi - |\theta_i - \theta_{i-1}| \tag{7c,d}$$

for $i = 2, 3, \ldots, n$.

5.2 Fixed obstacles

Suppose the workspace is cluttered with fixed spherical and rod shaped obstacles with a-priori *known* positions and sizes. For the entire robot to avoid a fixed obstacle, it is important that every point on the four sides (front, rear, right and left) of the car and every point on the n-links avoid the obstacles. We utilise the minimum distance technique (MDT) proposed by Sharma et al. (2012, 2015). The basic idea is to find a point on each component (the four sides of the car and the links) of the mobile robot that is closest to an obstacle. At any time $t \geq 0$, only the closest point on each component (and hence the entire robot) will avoid the obstacle.

5.2.1 Spherical obstacles

Now fix $q \in \mathbb{N}$ spherical obstacles within the boundaries of the workspace. The definition of these obstacles is given below.

Definition 5.1: The lth obstacle (for $l = 1, 2, \ldots, q$) is a sphere with centre (o_{l1}, o_{l2}, o_{l3}) and radius ro_l and is defined as the set

$$FO_l = \{(z_1, z_2, z_3) \in \mathbb{R}^3 : (z_1 - o_{l1})^2 + (z_2 - o_{l2})^2 + (z_3 - o_{l3})^2 \leq ro_l^2\}.$$

For the mobile manipulator to avoid an obstacle, points on each side of the mobile platform and on each link that are closest to the obstacle are found, where MDT is used to minimise the

distance function

$$D_{il} = \|(x^*_{il}, y^*_{il}, z^*_{il}) - (o_{l1}, o_{l2}, o_{l3})\|,$$

(for $i = 1, 2, \ldots, n+4$ and $l = 1, 2, \ldots, q$) where

$$\begin{aligned}
(x^*_{1l}, y^*_{1l}, z^*_{1l}) &= \left(x_0 + \frac{\ell_0 + 2\epsilon}{2}\cos\vartheta + \lambda_{1l} w \sin\vartheta, y_0 \right.\\
&\quad \left. + \frac{\ell_0 + 2\epsilon}{2}\sin\vartheta - \lambda_{1l} w \cos\vartheta, \lambda_0 a\right)\\
(x^*_{2l}, y^*_{2l}, z^*_{2l}) &= \left(x_0 - \frac{\ell_0 + 2\epsilon}{2}\cos\vartheta + \lambda_{1l} w \sin\vartheta, y_0 \right.\\
&\quad \left. - \frac{\ell_0 + 2\epsilon}{2}\sin\vartheta - \lambda_{1l} w \cos\vartheta, \lambda_0 a\right)\\
x^*_{3l}, y^*_{3l}, z^*_{3l}) &= \left(x_0 + \frac{w}{2}\sin\vartheta + \lambda_{2l}(\ell_0 + 2\epsilon)\cos\vartheta, y_0 \right.\\
&\quad \left. - \frac{w}{2}\cos\vartheta + \lambda_{2l}(\ell_0 + 2\epsilon)\sin\vartheta, \lambda_0 a\right)\\
(x^*_{4l}, y^*_{4l}, z^*_{4l}) &= \left(x_0 - \frac{w}{2}\sin\vartheta + \lambda_{2l}(\ell_0 + 2\epsilon)\cos\vartheta, y_0 \right.\\
&\quad \left. + \frac{w}{2}\cos\vartheta + \lambda_{2l}(\ell_0 + 2\epsilon)\sin\vartheta, \lambda_0 a\right)\\
(x^*_{4+i\,l}, y^*_{4+i\,l}, z^*_{4+i\,l}) &= (x_{i-1} + \lambda_{2+i\,l}\ell_i \cos\theta_i \cos(\theta_0 + \vartheta),\\
&\quad y_{i-1} + \lambda_{2+i\,l}\ell_i \cos\theta_i \sin(\theta_0 + \vartheta),\\
&\quad z_{i-1} + \lambda_{2+i\,l}\ell_i \sin\theta_i),
\end{aligned}$$

to obtain

$$\begin{aligned}
\lambda_{0l} &= \min\left\{1, \max\left\{0, \frac{o_{l3}}{a}\right\}\right\};\\
\lambda_{1l} &= \min\left\{\frac{1}{2}, \max\left\{-\frac{1}{2},\right.\right.\\
&\quad \left.\left.\frac{1}{w}[(x_0 - o_{l1})\sin\vartheta + (y_0 - o_{l2})\cos\vartheta]\right\}\right\};\\
\lambda_{2l} &= \min\left\{\frac{1}{2}, \max\left\{-\frac{1}{2},\right.\right.\\
&\quad \left.\left.\frac{1}{\ell_0 + 2\epsilon}[(o_{l1} - x_0)\cos\vartheta + (o_{l2} - y_0)\sin\vartheta]\right\}\right\};\\
\lambda_{2+i\,l} &= \min\left\{1, \max\left\{0, \frac{1}{\ell_i}\left[(o_{l1} - x_0)\cos(\vartheta + \theta_0)\right.\right.\right.\\
&\quad \left.\left. + (o_{l2} - y_0)\sin(\vartheta + \theta_0) - \sum_{j=1}^{i-1}\ell_j \cos\theta_j\right]\cos\theta_i\right.\\
&\quad \left.\left. + \frac{1}{\ell_i}\left[o_{l3} - a - \sum_{j=1}^{i-1}\ell_j \sin\theta_j \sin\theta_i\right]\right\}\right\}.
\end{aligned}$$

For the avoidance of the spherical obstacles by the mobile robot, the following avoidance functions are constructed:

$$W_{il}(\mathbf{x}) = \tfrac{1}{2}[(x^*_{il} - o_{l1})^2 + (y^*_{il} - o_{l2})^2 + (z^*_{il} - o_{l3})^2 - ro_l^2], \tag{8}$$

for $l = 1, 2, \ldots, q$ and $i = 1, 2, \ldots, n+4$.

5.2.2 Rod obstacles

Suppose that there are $m \in \mathbb{N}$ stationary rod objects in the workspace which the robot potentially has to avoid enroute its target. The following definition is considered:

Definition 5.2: The kth stationary rod is a straight solid object with endpoints at (a_{k1}, a_{k2}, a_{k3}) and (b_{k1}, b_{k2}, b_{k3}) and is defined as the set

$$\begin{aligned}
CO_k = \{(z_1, z_2, z_3) \in \mathbb{R}^3 : &(z_1 - a_{k1} - \gamma_k(b_{k1} - a_{k1}))^2\\
&+ (z_2 - a_{k2} - \gamma_k(b_{k2} - a_{k2}))^2\\
&+ (z_3 - a_{k3} - \gamma_k(b_{k3} - a_{k3}))^2 \le r_k^2\}
\end{aligned}$$

where $2r_k$ is cross-sectional diameter of the rod and $\gamma_k \in [0, 1]$.

For avoidance, we need to find two sets of points (one on each body of the mobile robot and the other on each rod) such that the two sets are closest to each other. For this, again MDT is utilised to minimise the distance function

$$D^*_{ik} = \|(x^{**}_{ik}, y^{**}_{ik}, z^{**}_{ik}) - (X_{ik}, Y_{ik}, Z_{ik})\|$$

where

$$\begin{aligned}
(X_{ik}, Y_{ik}, Z_{ik}) &= (a_{k1} + \gamma_{ik}(b_{k1} - a_{k1}), a_{k2}\\
&\quad + \gamma_{ik}(b_{k2} - a_{k2}), a_{k3} + \gamma_{ik}(b_{k3} - a_{k3}))\\
(x^{**}_{1k}, y^{**}_{1k}, z^{**}_{1k}) &= \left(x_0 + \frac{\ell_0 + 2\epsilon}{2}\cos\vartheta + \lambda^*_{1k} w \sin\vartheta, y_0 \right.\\
&\quad \left. + \frac{\ell_0 + 2\epsilon}{2}\sin\vartheta - \lambda^*_{1k} w \cos\vartheta, \lambda^*_0 a\right)\\
(x^{**}_{2k}, y^{**}_{2k}, z^{**}_{2k}) &= \left(x_0 - \frac{\ell_0 + 2\epsilon}{2}\cos\vartheta + \lambda^*_{1k} w \sin\vartheta, y_0 \right.\\
&\quad \left. - \frac{\ell_0 + 2\epsilon}{2}\sin\vartheta - \lambda^*_{1k} w \cos\vartheta, \lambda^*_0 a\right)\\
(x^{**}_{3k}, y^{**}_{3k}, z^{**}_{3k}) &= \left(x_0 + \frac{w}{2}\sin\vartheta \right.\\
&\quad + \lambda^*_{2k}(\ell_0 + 2\epsilon)\cos\vartheta, y_0\\
&\quad \left. - \frac{w}{2}\cos\vartheta + \lambda^*_{2k}(\ell_0 + 2\epsilon)\sin\vartheta, \lambda^*_0 a\right)\\
(x^{**}_{4k}, y^{**}_{4k}, z^{**}_{4k}) &= \left(x_0 - \frac{w}{2}\sin\vartheta + \lambda^*_{2k}(\ell_0 + 2\epsilon)\cos\vartheta, \right.\\
&\quad y_0 + \frac{w}{2}\cos\vartheta\\
&\quad \left. + \lambda^*_{2k}(\ell_0 + 2\epsilon)\sin\vartheta, \lambda^*_0 a\right)\\
(x^{**}_{4+i\,k}, y^{**}_{4+i\,k}, z^{**}_{4+i\,k}) &= (x_{i-1} + \lambda^*_{2+i\,k}\ell_i \cos\theta_i \cos(\theta_0 + \vartheta),\\
&\quad y_{i-1} + \lambda^*_{2+i\,k}\ell_i \cos\theta_i \sin(\theta_0 + \vartheta),\\
&\quad z_{i-1} + \lambda^*_{2+i\,k}\ell_i \sin\theta_i),\\
&\quad i = 1, 2, \ldots, n.
\end{aligned}$$

The parameters γ_{ik}, λ^*_{1k}, λ^*_{2k} and $\lambda^*_{2+i\,k}$ for which D^*_{ik} is minimum are given in the Appendix. For the avoidance of the rod obstacles, we construct the potential functions

$$R_{ik}(\mathbf{x}) = \tfrac{1}{2}[(x^{**}_{ik} - X_{ik})^2 + (y^{**}_{ik} - Y_{ik})^2 + (z^{**}_{ik} - Z_{ik})^2 - r_k^2], \tag{9}$$

for $k = 1, 2, \ldots, m$ and $i = 1, 2, \ldots, n+4$.

5.3 Workspace restrictions

The three-dimensional workspace is a fixed, closed and bounded cuboid region, defined, for some constants η_1, η_2, and η_3 as

$$WS = \{(z_1, z_2, z_3) \in \mathbb{R}^3 : -\eta_1 \leq z_1 \leq \eta_1, \\ -\eta_2 \leq z_2 \leq \eta_2, 0 \leq z_3 \leq \eta_3\}.$$

We require the mobile manipulator to stay within the 3D workspace at all time $t \geq 0$. As such, we construct the potential function

$$B_{i1}(\mathbf{x}) = x_i + \eta_1, \quad B_{i2}(\mathbf{x}) = \eta_1 - x_i, \tag{10a,b}$$

$$B_{i3}(\mathbf{x}) = y_i + \eta_2, \quad B_{i4}(\mathbf{x}) = \eta_2 - y_i, \tag{10c,d}$$

$$B_{i5}(\mathbf{x}) = z_i, \quad B_{i6}(\mathbf{x}) = \eta_3 - z_i, \tag{10e,f}$$

for $i = 1, 2, \ldots, n$ and for the mobile platform we have

$$H_1(\mathbf{x}) = x_0 + \frac{\ell_0 + 2\epsilon}{2}\cos\vartheta + \frac{w}{2}\sin\vartheta + \eta_1, \tag{11a}$$

$$H_2(\mathbf{x}) = \eta_1 - x_0 - \frac{\ell_0 + 2\epsilon}{2}\cos\vartheta - \frac{w}{2}\sin\vartheta, \tag{11b}$$

$$H_3(\mathbf{x}) = y_0 + \frac{\ell_0 + 2\epsilon}{2}\sin\vartheta - \frac{w}{2}\cos\vartheta + \eta_2, \tag{11c}$$

$$H_4(\mathbf{x}) = \eta_2 - y_0 - \frac{\ell_0 + 2\epsilon}{2}\sin\vartheta + \frac{w}{2}\cos\vartheta, \tag{11d}$$

$$H_5(\mathbf{x}) = x_0 - \frac{\ell_0 + 2\epsilon}{2}\cos\vartheta + \frac{w}{2}\sin\vartheta + \eta_1, \tag{11e}$$

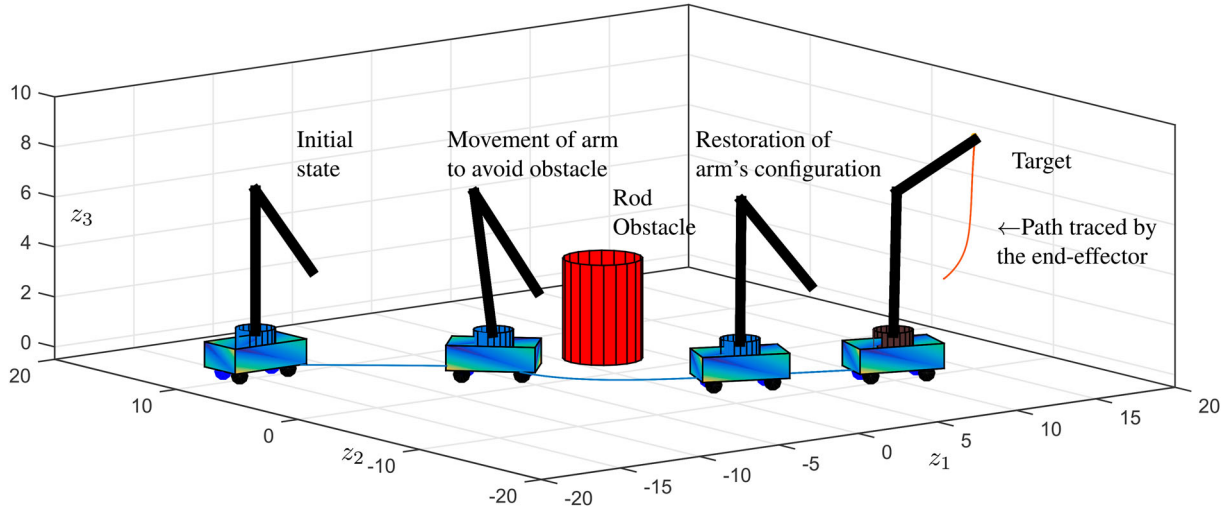

Figure 3. Trajectory of the two-link mobile manipulator with $\mathbf{x}_0(0) = (-15, 10)$, $\mathbf{e}_0 = (10, -10)$ and $\mathbf{e}_a = (15, -10, 8.8)$ in Scenario 1.

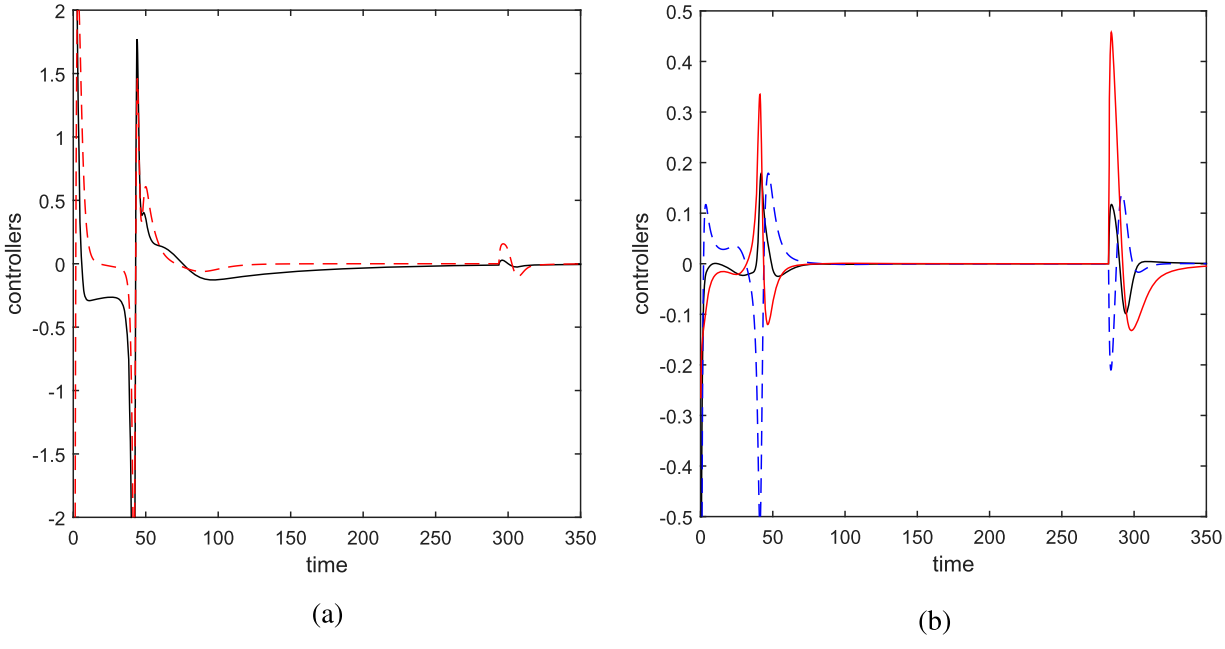

Figure 4. Evolution of the nonlinear controllers along the trajectory shown in Scenario 1: (a) Controllers ρ_1 in black, ρ_2 in red and (b) controllers σ_0 in black, σ_1 in blue and σ_2 in red.

$$H_6(\mathbf{x}) = \eta_1 - x_0 + \frac{\ell_0 + 2\epsilon}{2}\cos\vartheta - \frac{w}{2}\sin\vartheta, \tag{11f}$$

$$H_7(\mathbf{x}) = y_0 - \frac{\ell_0 + 2\epsilon}{2}\sin\vartheta - \frac{w}{2}\cos\vartheta + \eta_2, \tag{11g}$$

$$H_8(\mathbf{x}) = \eta_2 - y_0 + \frac{\ell_0 + 2\epsilon}{2}\sin\vartheta + \frac{w}{2}\cos\vartheta. \tag{11h}$$

6. Design of the nonlinear control laws

This section defines a Lyapunov function for system (3) and the nonlinear control laws are designed. Furthermore, the stability issues pertaining to system (3) are discussed and a proof of obstacle avoidance scheme is provided.

6.1 Lyapunov function

A Lyapunov function is defined by combining all the potential functions (4)–(11) and introducing *control parameters*, $\alpha_i > 0$, $\beta_i > 0, \zeta_{il} > 0, \xi_{ik} > 0, \varsigma_{ir} > 0$ and $\mu_s > 0$ where $i, l, k, r, s \in \mathbb{N}$. This Lyapunov function or total potentials for system (3) is as follows:

$$\begin{aligned} L(\mathbf{x}) = \sum_{j=1}^{3} V_j(\mathbf{x}) + G(\mathbf{x}) \Bigg[& \sum_{i=1}^{n+3} \frac{\alpha_i}{U_i(\mathbf{x})} + \sum_{i=1}^{2n} \frac{\beta_i}{S_i(\mathbf{x})} \\ & + \sum_{i=1}^{n+4} \left(\sum_{l=1}^{q} \frac{\zeta_{il}}{W_{il}(\mathbf{x})} + \sum_{k=1}^{m} \frac{\xi_{ik}}{R_{ik}(\mathbf{x})} \right) \\ & + \sum_{i=1}^{n} \sum_{r=1}^{6} \frac{\varsigma_{ir}}{B_{ir}(\mathbf{x})} + \sum_{s=1}^{8} \frac{\mu_s}{H_s(\mathbf{x})} \Bigg] \end{aligned} \tag{12}$$

where

$$\begin{aligned} G(\mathbf{x}) = & \frac{1}{2}[(x_0 - \tau_1)^2 + (y_0 - \tau_2)^2] \\ & + \frac{h_c}{2}[(x - p_1)^2 + (y - p_2)^2 + (z - p_3)^2] \end{aligned}$$

is an auxiliary function required for the Lyapunov function to vanish at the target. The Lyapunov function is positive, continuous and bounded over the domain

$$\begin{aligned} D = \{ & \mathbf{x} \in \mathbb{R}^{2n+7} : \ U_i(\mathbf{x}) > 0, \ W_{il}(\mathbf{x}) > 0, R_{ik}(\mathbf{x}) > 0, \\ & B_{ir}(\mathbf{x}) > 0, \ H_s(\mathbf{x}) > 0, \ 0 < \theta_1 < \pi, \\ & 0 < |\theta_i - \theta_{i-1}| < \pi \}. \end{aligned}$$

A unique and essential feature of the Lyapunov function lies in its control parameters. The control parameters, $\alpha_i > 0$, $\beta_i > 0$, $\zeta_{il} > 0$, $\xi_{ik} > 0$, $\varsigma_{ir} > 0$ and $\mu_s > 0$, which are determined using the brute force method, increase the freedom of manoeuvrability of the mobile manipulator to better account for the obstacles. For example, a relatively larger value of ζ_{il} will enable to ith component of the manipulator to avoid the lth obstacle from a greater distance.

6.2 Control laws

Suppose ϑ^* is the orientation of the mobile platform at the pseudo-target. Let θ_0^* and θ_i^*, respectively, be the orientations of the rotatable base and the ith link when the end-effector reaches its target. The point $\mathbf{e} = (\tau_1, \tau_2, \vartheta^*, 0, 0, \theta_0^*, \theta_1^*, \ldots, \theta_n^*, 0, 0, \ldots, 0)$ is an equilibrium point of system (3). We now design the control laws such that $\mathbf{e}$ is a stable equilibrium point. This is provided in Theorem 6.1.

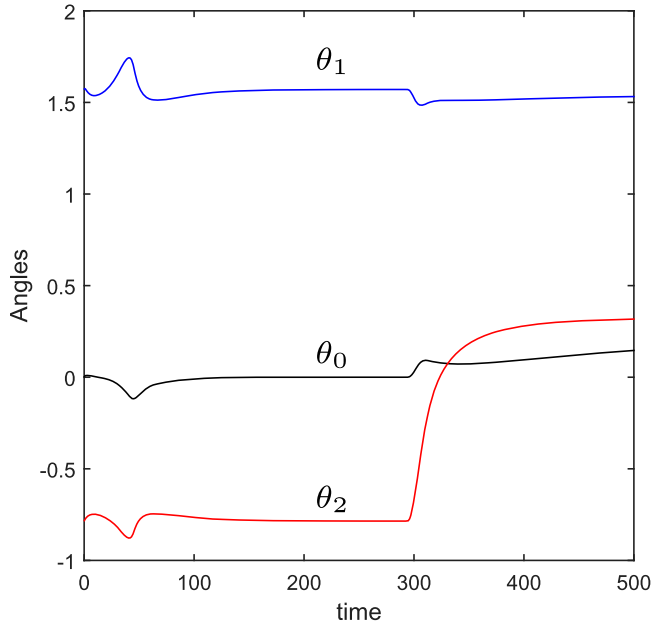

Figure 5. Evolution of the orientations of the links (θ_0 in black, θ_1 in blue and θ_2 in red) along the trajectory shown in Scenario 1.

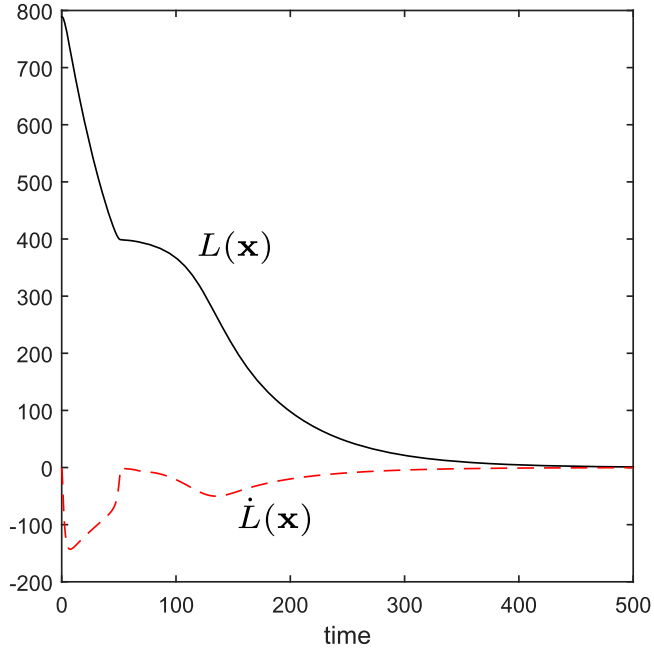

Figure 6. Evolution of the Lyapunov function $L(\mathbf{x})$ and its time derivative $\dot{L}(\mathbf{x})$ along the trajectory shown in Scenario 1.

Theorem 6.1: *The equilibrium point* $\mathbf{e} = (\tau_1, \tau_2, \vartheta^*, 0, 0, \theta_0^*, \theta_1^*, \ldots, \theta_n^*, 0, 0, \ldots, 0)$ *of system* (3) *is stable provided the controllers* ρ_1, ρ_2 *and* σ_i $(i = 0, 1, \ldots, n)$ *are defined as*

$$\left.\begin{aligned}
\rho_1 &= -\left(\delta_1 v + \frac{\partial L}{\partial x_0}\cos\vartheta + \frac{\partial L}{\partial y_0}\sin\vartheta\right) \Big/ \left(1 + G\frac{\alpha_1}{U_1^2}\right), \\
\rho_2 &= -\left(\delta_2 \varpi - \frac{\partial L}{\partial x_0}\frac{\ell_0}{2}\sin\vartheta \right. \\
&\quad \left. + \frac{\partial L}{\partial y_0}\frac{\ell_0}{2}\cos\vartheta + \frac{\partial L}{\partial \vartheta}\right) \Big/ \left(1 + G\frac{\alpha_2}{U_2^2}\right), \\
\sigma_i &= -\left(\delta_{3+i}\omega_i + \frac{\partial L}{\partial \theta_i}\right) \Big/ \left(1 + G\frac{\alpha_{3+i}}{U_{3+i}^2}\right),
\end{aligned}\right\} \tag{13}$$

where $\delta_1 > 0$, $\delta_2 > 0$, $\delta_{3+i} > 0$ $(i = 0, 1, \ldots, n)$ *are called the convergence parameters.*

Proof: Note that the Lyapunov function $L(\mathbf{x})$ defined in (12) is continuous, positive and bounded over the domain D. Moreover, $L(\mathbf{e}) = 0$ and $L(\mathbf{x}) > 0$ for all $\mathbf{x} \neq \mathbf{e}$. On the domain D, $L(\mathbf{x})$ has continuous first partial derivatives, and therefore

$$\begin{aligned}
\dot{L}(\mathbf{x}) &= \frac{\partial L}{\partial x_0}\dot{x}_0 + \frac{\partial L}{\partial y_0}\dot{y}_0 + \frac{\partial L}{\partial \vartheta}\dot{\vartheta} + \sum_{i=0}^{n}\frac{\partial L}{\partial \theta_i}\dot{\theta}_i \\
&\quad + \frac{\partial L}{\partial v}\dot{v} + \frac{\partial L}{\partial \varpi}\dot{\varpi} + \sum_{i=0}^{n}\frac{\partial L}{\partial \omega_i}\dot{\omega}_i \\
&= \left[\frac{\partial L}{\partial x_0}\cos\vartheta + \frac{\partial L}{\partial y_0}\sin\vartheta + \rho_1\left(1 + G\frac{\alpha_1}{U_1^2}\right)\right] v \\
&\quad + \left[-\frac{\partial L}{\partial x_0}\frac{\ell_0}{2}\sin\vartheta + \frac{\partial L}{\partial y_0}\frac{\ell_0}{2}\cos\vartheta + \frac{\partial L}{\partial \vartheta}\right. \\
&\quad \left. + \rho_2\left(1 + G\frac{\alpha_2}{U_2^2}\right)\right]\varpi \\
&\quad + \sum_{i=0}^{n}\left[\frac{\partial L}{\partial \theta_i} + \sigma_i\left(1 + G\frac{\alpha_{3+i}}{U_{3+i}^2}\right)\right]\omega_i
\end{aligned}$$

Substituting ρ_1, ρ_2 and σ_i from (13), we obtain

$$\dot{L}(\mathbf{x}) = -\delta_1 v^2 - \delta_2 \varpi^2 - \sum_{i=0}^{n}\delta_{3+i}\omega_i^2 \leq 0.$$

It is clear that in the domain D, $\dot{L}(\mathbf{x}) \leq 0$ and $\dot{L}(\mathbf{e}) = 0$. Hence we conclude that $\mathbf{e}$ is a stable equilibrium point of system (3). ■

7. Computer simulation

In this section, we demonstrate computer simulations of the mobile manipulator with different number of links in an obstacle ridden three-dimensional workspace. The three scenarios given in this section capture realistic situations to illustrate

Table 1. Values of the different parameters used in Scenario 2.

Initial and final configuration	
Initial position (ft)	$\mathbf{x}_0(0) = (-15, 10)$.
Initial angular positions (rad)	$\vartheta(0) = 0, \theta_0(0) = 0, \theta_1(0) = \frac{\pi}{2}, \theta_2(0) = -\frac{\pi}{4}$.
Final positions (ft)	$\mathbf{e}_0 = (15, -15)$ and $\mathbf{e}_a = (18, -18, 8.8)$
Robot parameters	
Platform dimensions (ft)	$\ell_0 = 5, w = 4.3, \epsilon = 1, a = 1$.
Link dimensions (ft)	$\ell_1 = 5, \ell_2 = 5$.
Obstacle parameters	
Rod 1	(2, −8, 0) - (2, −8, 4)
Rod 2	(2, 10, 0) - (2, 10, 4)
Rod 3	(2, −8, 4) - (2, 10, 4)
Other parameters	
Workspace dimensions	$-20 \leq z_1 \leq 20, -20 \leq z_2 \leq 20, 0 \leq z_3 \leq 10$
Convergence parameters	$\delta_i = 10$ for $i = 1, \ldots, 5$
Control parameters	$\alpha_i = 0.1$ for $i = 1, 2, \ldots, 5$. $\beta_i = 0.1$ for $i = 1, 2, \ldots, 4$ $\xi_{ik} = 0.5$ for $i = 1, 2, \ldots, 6$ and $k = 1, 2, 3$ $\varsigma_{ir} = 0.1$ for $i = 1, 2$ and $r = 1, 2, \ldots, 6$. $\mu_s = 0.1$ for $s = 1, 2, \ldots, 8$

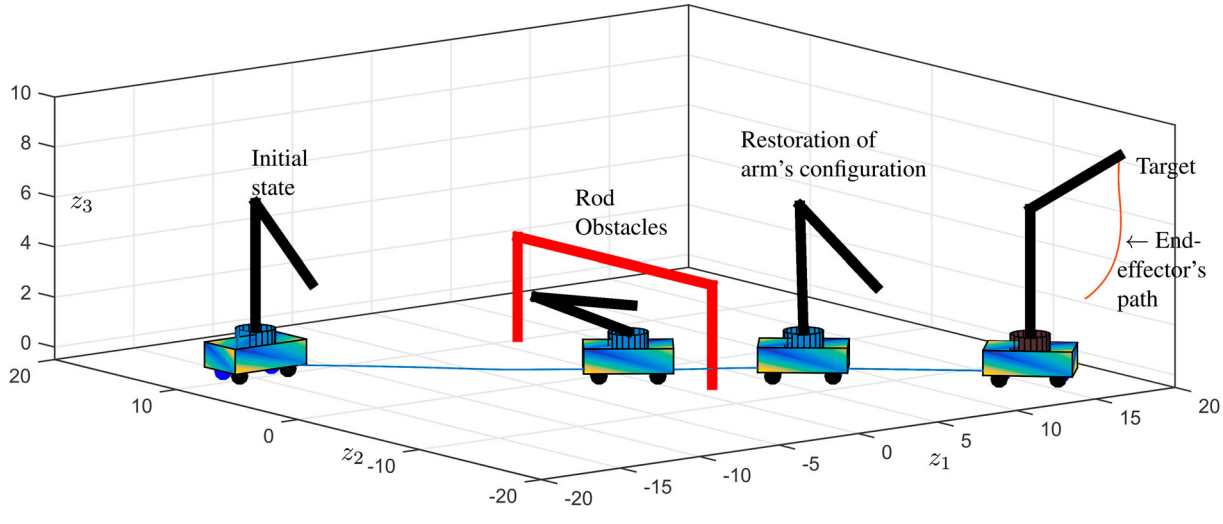

Figure 7. Trajectory of the two-link mobile manipulator in Scenario 2. Path traced by the centre of the platform is shown in blue and path traced by the end-effector is shown in red.

the effectiveness and robustness of the acceleration-based controllers and the control scheme.

7.1 Scenario 1

Figure 3 shows the trajectory of the three-dimensional two-link mobile manipulator from an initial to the final position. As governed by step 1 of the two-step algorithm, the mobile robot successfully moves from the initial position to the pseudo-target whilst avoiding a rod-shaped obstacle, without any attraction of the end-effector to its target. In step 2, when the mobile platform is within a distance of $c = 1$ *ft* from its pseudo-target, the end-effector is subsequently seen to be attracted to its target. It can also be noticed that there is a temporary distortion of the manipulator's configuration when the robot approaches the obstacle. This is due to the unique form of the attractive potential function $V_2(x)$ given in (4b). However, when the robot moves past the obstacle, the arm's initial configuration is restored. The initial and final positions and other simulation details are given below.

1. *Robot parameters* (*ft*): $\ell_0 = 5, w = 4.3, \epsilon = 1, a = 1, \ell_1 = 6, \ell_2 = 6$.
2. *Initial and final positions* (*ft*): $\mathbf{x}_0(0) = (-15, 10)$, $\mathbf{e}_0 = (10, -10)$, $\mathbf{e}_a = (15, -10, 8.8)$.
3. *Angular positions* (*rad*): $\vartheta(0) = 0$, $\theta_0(0) = 0$, $\theta_1(0) = \frac{\pi}{2}$, $\theta_2(0) = -\frac{\pi}{4}$.
4. *Fixed rod obstacle* (*ft*): Dimension: (0, 3, 0) - (0, 3, 4). Cross-sectional diameter: 4.
5. *Physical limitations*: $v_{\max} = 5$ *ft*/*s*, $\phi_{\max} = 70^\circ$ and $u_{\max} = 1$ *rad*/*s*.
6. *Convergence parameters*: $\delta_i = 10$ for $i = 1, \ldots, 5$.

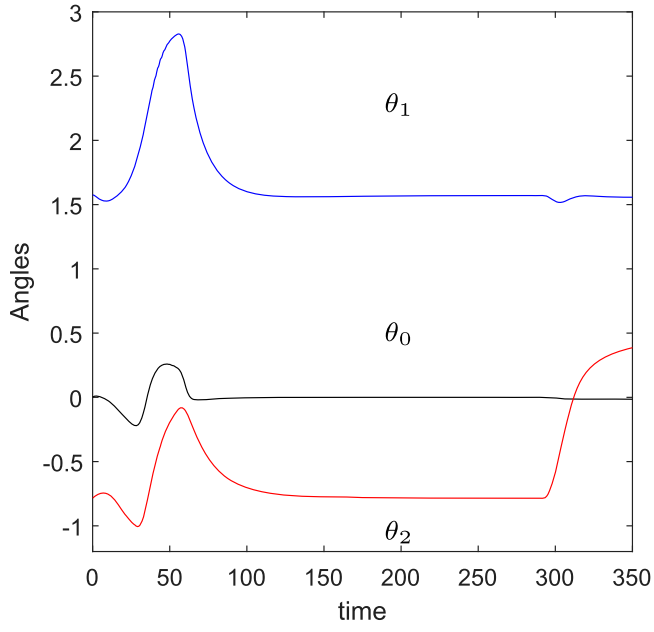

Figure 9. Evolution of the orientations of the links (θ_0 in black, θ_1 in blue and θ_2 in red) along the trajectory shown in Scenario 2.

7. *Control parameters*:

Control parameter for:	Value of the parameter
Artificial obstacles	$\alpha_i = 0.01$ for $i = 1, 2, \ldots, 5$
	$\beta_i = 0.01$ for $i = 1, 2, \ldots, 4$
Fixed obstacles	$\xi_{i1} = 0.5$ for $i = 1, 2, \ldots, 6$
Workspace restrictions	$\varsigma_{ir} = 0.1$ for $i = 1, 2$ and $r = 1, 2, \ldots, 6$
	$\mu_s = 0.1$ for $s = 1, 2, \ldots, 8$

8. *Workspace boundaries* (*ft*): $\eta_1 = 20$, $\eta_2 = 20$ and $\eta_3 = 10$.
9. *Other parameters*: $c = 1, \kappa = 5$.

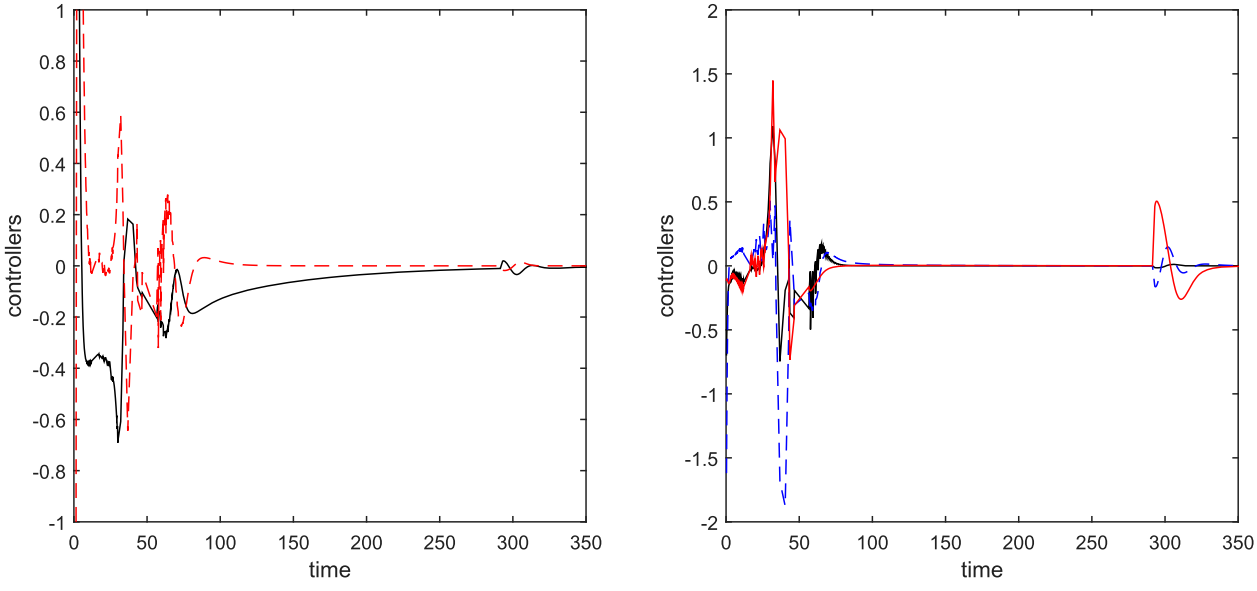

Figure 8. Evolution of nonlinear controllers along the trajectory shown in Scenario 2: (a) controllers ρ_1 in black, ρ_2 in red and (b) controllers σ_0 in black, σ_1 in blue and σ_2 in red.

The behaviour of the nonlinear acceleration-based controllers along the trajectory of the mobile manipulator is shown in Figure 4. One can clearly notice the convergence of the controllers at the final state implying the effectiveness of the new controllers. The graphs of θ_0, θ_1 and θ_2 are also shown in Figure 5. The change of orientations between $t = 40$ to $t = 60$ units indicates the movement of the arm to avoid the rod-shaped obstacles. The almost flat portions after $t = 60$ units indicate the restoration of the arm's configuration after avoiding the obstacle. The change of orientations after $t = 300$ units was due to the convergence of the end-effector to the target. Figure 6 shows the evolution of the Lyapunov function and its time derivative along the system trajectory. Not only do the graphs verify the stability property of system (3), but they also provide information where the mobile robot has accelerated or decelerated. An increase in $\dot{L}(\mathbf{x})$ indicates that the robot is decelerating, whereas a decrease in $\dot{L}(\mathbf{x})$ indicates that the robot is accelerating.

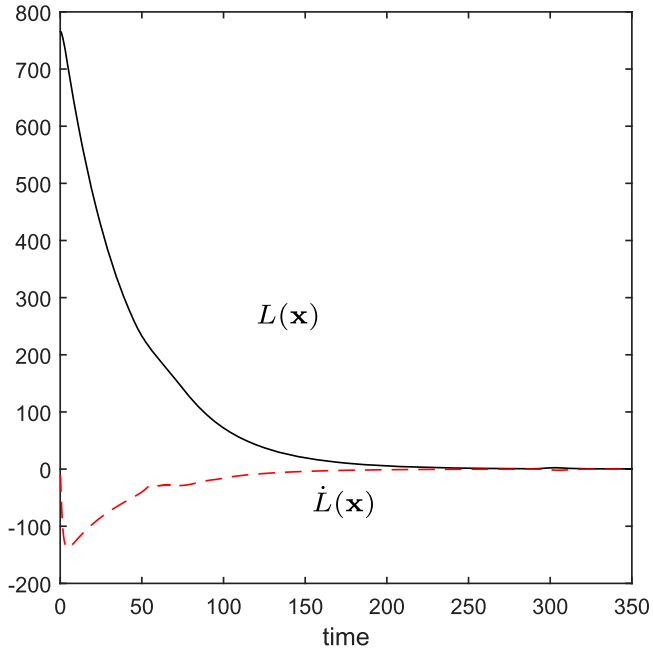

Figure 10. Evolution of the Lyapunov function $L(\mathbf{x})$ and its time derivative $\dot{L}(\mathbf{x})$ along the trajectory shown in Scenario 2.

7.2 Scenario 2

Scenario 2 considers a two-link mobile manipulator manoeuvring from initial to final states, whilst avoiding collisions with three rod-shaped obstacles pre-arranged into a low-rising bar as shown in Figure 7. The values of different parameters required for the simulation are listed under Table 1.

The results of the two-step algorithm is clearly illustrated in the figure. We note that the two-link arm behave in unique ways to avoid the rod-shaped bar. The changes of the arm's angular orientations are observed when the arm approaches and subsequently avoids the bar in its path. However, the initial state of the arm is re-achieved after the avoidance due to the unique and tailored form of the potential function given in (5).

Figure 8 shows explicitly the time evolution of the relevant controllers along the trajectory of the mobile manipulator. We notice the convergence of the controllers at the final state implying the effectiveness of the new controllers. The evolution of the Lyapunov function and its time derivative are shown in Figure 10. The graphs of θ_0, θ_1 and θ_2 are shown in Figure 9. The change of orientations between $t = 30$ to $t = 70$ units indicates the movement of the arm to avoid the rod-shaped obstacles. The almost flat portions after $t = 70$ units indicate the restoration of the arm's configuration after avoiding the obstacle. The change of orientations after $t = 300$ units was due to the convergence of the end-effector to the target.

7.3 Scenario 3

Scenario 3 simulates another interesting situation with a four-link mobile manipulator manoeuvring as shown in Figure 11.

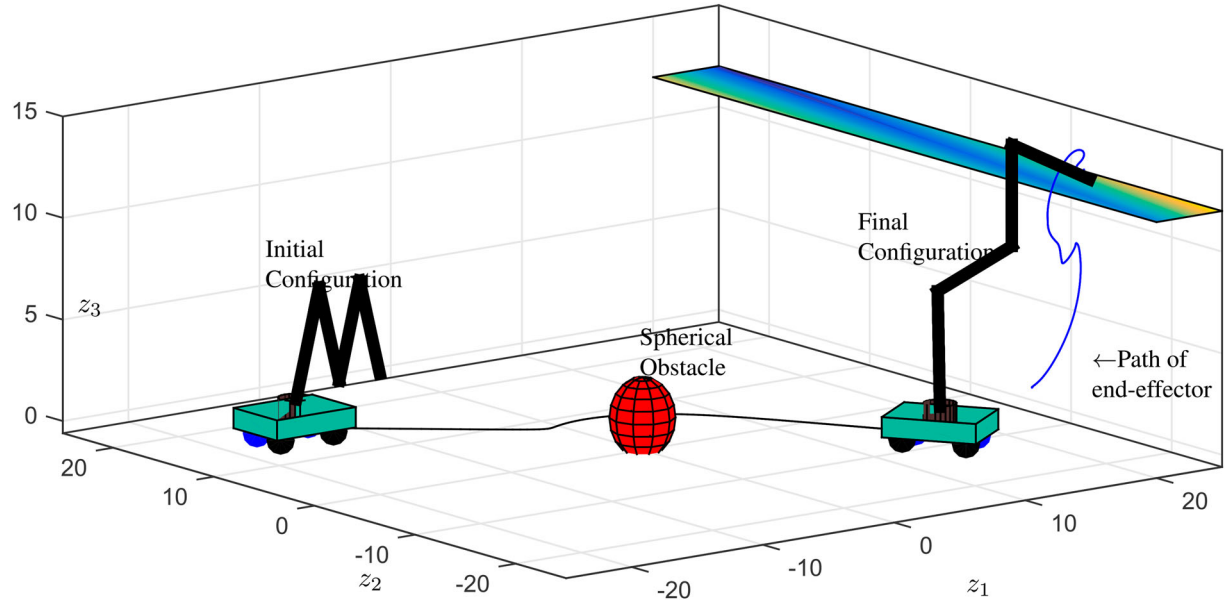

Figure 11. Trajectory of the four-link mobile manipulator in Scenario 3.

Table 2. Values of the different parameters used in Scenario 3.

Initial and final configuration	
Initial position (ft)	$\mathbf{x}_0(0) = (-15, 15)$.
Initial angular positions (rad)	$\vartheta(0) = 0, \theta_0(0) = 0, \theta_1(0) = \frac{2\pi}{5}, \theta_2(0) = -\frac{2\pi}{5}, \theta_3(0) = \frac{2\pi}{5}, \theta_4(0) = -\frac{2\pi}{5}$.
Final positions (ft)	$\mathbf{e}_0 = (15, -10)$ and $\mathbf{e}_a = (22, -15, 12)$
Robot parameters	
Platform dimensions (ft)	$\ell_0 = 5, w = 4.3, \epsilon = 1, a = 1$.
Link dimensions (ft)	$\ell_1 = 5, \ell_2 = 5, \ell_3 = 5, \ell_4 = 5$.
Obstacle parameters	
Spherical obstacle dimension (ft)	Centre: (0,0,1), radius: 2
Shelf dimension (ft)	(25, 25, 12) - (25, −25, 12), width = 5
Other parameters	
Convergence parameters	$\delta_i = 10$ for $i = 1, \ldots, 5$
Control parameters	$\alpha_i = 0.1$ for $i = 1, 2, \ldots, 5$. $\beta_i = 0.1$ for $i = 1, 2, \ldots, 4$ $\zeta_{i1} = 0.5$ for $i = 1, 2, \ldots, 6$. $\xi_{ik} = 0.1$ for $i = 1, 2, \ldots, 8$ $\varsigma_{ir} = 0.1$ for $i = 1, 2$ and $r = 1, 2, \ldots, 6$. $\mu_s = 0.1$ for $s = 1, 2, \ldots, 8$

The values of different parameters required for the simulation are listed under Table 2.

This scenario captures a real-life situation of placing objects on a shelf, which is made up from an appropriate arrangement of multiple thin rods. The mobile manipulator avoided a spherical object en route the pseudo target, again with no attraction of the end-effector to its target. As indicated in step 2 of the two-step algorithm, the end-effector moves from underneath the shelf, avoids collision with the shelf and finally converges to its target (treated as the dropping-off area) just above the shelf. The behaviour of the non-linear controllers are similar to those shown in scenario 1 and 2. The graphs of θ_0, θ_1, θ_3, θ_4 and θ_5 are shown in Figure 12. The evolution of the Lyapunov function and its time derivative are shown in Figure 13.

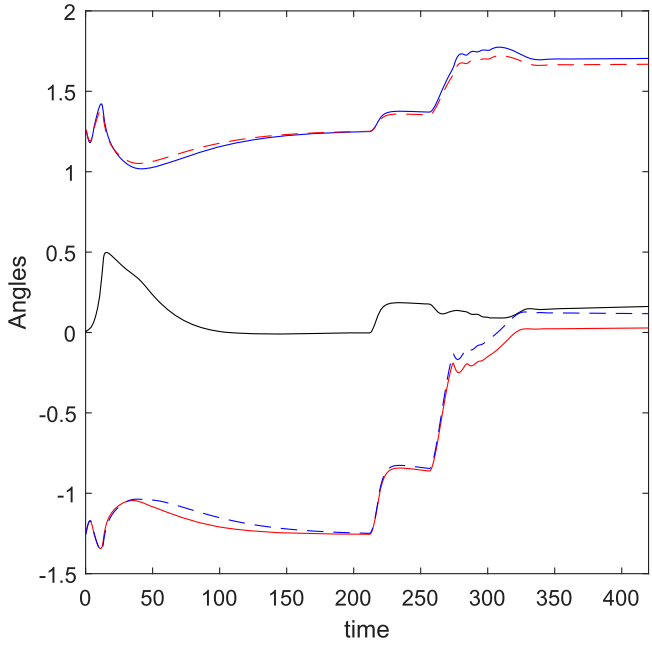

Figure 12. Evolution of the orientations of the links (θ_0 in black, θ_1 in blue, θ_2 in red, θ_4 in dashed red and θ_5 in dashed blue) along the trajectory shown in Scenario 3.

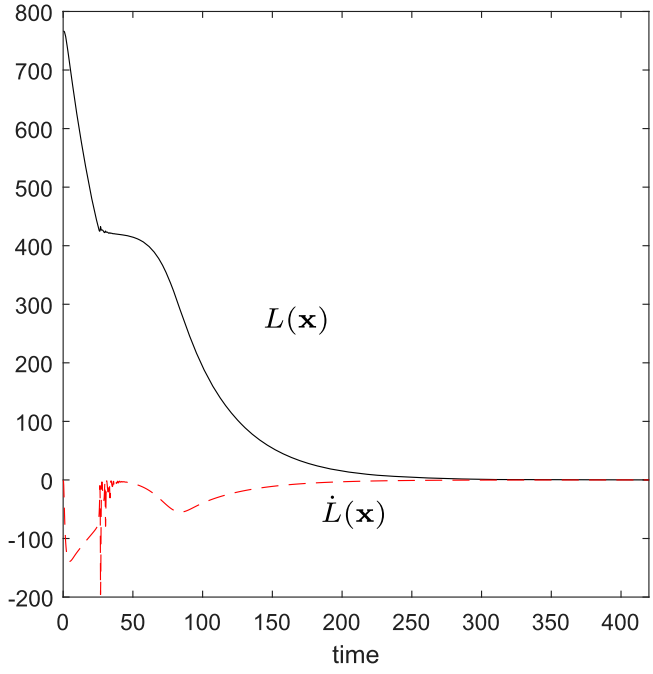

Figure 13. Evolution of the Lyapunov function $L(\mathbf{x})$ and its time derivative $\dot{L}(\mathbf{x})$ along the trajectory shown in Scenario 3.

8. Concluding remarks

In this paper, a new solution to the motion planning and control problem of a three-dimensional n-link mobile manipulator is proposed. The Lyapunov-based control scheme is utilised to control the motion of the mobile robot in a constrained three-dimensional workspace randomly fixed with spherical and rod-shaped obstacles of known sizes and positions. For obstacle avoidance, the Minimum Distance Technique was utilised where closest points from the four sides of the nonholonomic mobile platform and each n-link avoid obstacles.

For the first time in literature, a pseudo-target is designed as an attraction point for the nonholonomic mobile platform in a unique new two-step algorithm where the obstacle avoidance scheme is active for the complete mobile manipulator system. When the mobile platform is within some predefined distance away from the pseudo-target, the end-effector subsequently moves and converges to its designated target. The acceleration-based nonlinear control laws proposed also take into account all mechanical singularities and velocity limitations associated with n-link mobile manipulator system.

Future work in this area includes motion planning and control of mobile manipulators with prismatic links, mobile manipulators hitched to trailers, multiple mobile manipulators. Moreover, partially known or fully unknown workspace, where the positions, sizes and geometry of obstacles may be unknown, will be an interesting but challenging research to consider in future.

Disclosure statement

No potential conflict of interest was reported by the author(s).

ORCID

Avinesh Prasad http://orcid.org/0000-0003-4186-1053
Bibhya Sharma http://orcid.org/0000-0002-7519-7712
Jito Vanualailai http://orcid.org/0000-0003-0792-6220
Sandeep Kumar http://orcid.org/0000-0002-6951-4742

References

Assaf, M., Kumar, R., Nambiar, K., Narayan, S., Nath, N., Reddy, Y., Sharma, K., & Sharma, B. (2018). Enabling students with severe disabilities to communicate with learning environments. In *2018 5th Asia-Pacific World Congress on Computer Science and Engineering (APWC on CSE)* (pp. 201–206), Nadi, Fiji, IEEE.

Boukattaya, M., Damak, T., & Jallouli, M. (2011). Robust adaptive control for mobile manipulators. *International Journal of Automation and Computing*, *8*(1), 8–13. https://doi.org/10.1007/s11633-010-0548-y

Buizza Avanzini, G., Zanchettin, A. M., & Rocco, P. (2018). Constrained model predictive control for mobile robotic manipulators. *Robotica*, *36*(1), 19–38. https://doi.org/10.1017/S0263574717000133

Bunjaku, D., Stankovski, J., & Stankovski, M. (2017). Dynamic modelling and asymptotic point stabilization control of two differential wheeled mobile robot. *Journal of Electrical Engineering and Information Technologies*, *1*(1–2), 25–35.

Cao, Y., Yu, W., Ren, W., & Chen, G. (2013). An overview of recent progress in the study of distributed multi-agent coordination. *IEEE Transactions on Industrial Informatics*, *9*(1), 427–438. https://doi.org/10.1109/TII.2012.2219061

Chen, J. Y., & Barnes, M. J. (2012). Supervisory control of multiple robots in dynamic tasking environments. *Ergonomics*, *55*(9), 1043–1058. https://doi.org/10.1080/00140139.2012.689013

Chevalier, A., Bossche, M., Copot, C., & De Keyser, R. (2014). Formation control strategies for emulation of field covering. In *Proceedings of the 18th International Conference on System Theory, Control and Computing* (pp. 526–531), Sinaia, Romania. IEEE.

Chung, J. H., & S. A. Velinsky (1998). Modeling and control of a mobile manipulator. *Robotica*, *16*(6), 607–613. https://doi.org/10.1017/S0263574798000873

Cui, R., Sam Ge, S., Voon Ee How, B., & Sang Choo, Y. (2010). Leader–follower formation control of underactuated autonomous underwater vehicles. *Ocean Engineering*, *37*(17–18), 1491–1502. https://doi.org/10.1016/j.oceaneng.2010.07.006

Djebrani, S., Benali, A., & Abdessemed, F. (2012). Modelling and control of an omnidirectional mobile manipulator. *International Journal of Applied Mathematics and Computer Science*, *22*(3), 601–616. https://doi.org/10.2478/v10006-012-0046-1

Hamner, B., Koterba, S. C., Shi, J., Simmons, R., & Singh, S. (2010). An autonomous mobile manipulator for assembly tasks. *Autonomous Robots*, *28*(1), 131–149. https://doi.org/10.1007/s10514-009-9142-y

Hootsmans, N. A. M., & Dubowsky, S. (1991). Large motion control of mobile manipulators including vehicle suspension characteristics. In *IEEE International Conference on Robotics and Automation* (pp. 2336–2341), Sacramento, CA, USA. IEEE.

Jaulin, L., & Le Bars, F. (2013). An interval approach for stability analysis: Application to sailboat robotics. *IEEE Transactions on Robotics*, *29*(1), 282–287. https://doi.org/10.1109/TRO.2012.2217794

Khatib, O. (1986). Real-time obstacle avoidance for manipulators and mobile robots. *International Journal of Robotics Research*, *5*(1), 90–98. https://doi.org/10.1177/027836498600500106

Kumar, S. A., Vanualailai, J., Sharma, B., Chaudary, A., & Kapadia, V. (2016). Emergent formations of a lagrangian swarm of unmanned ground vehicles. In *Proceedings of the 2016 14th International Conference on Control, Automation, Robotics and Vision, ICARCV 2016*, Phuket, Thailand. IEEE.

Kumar, S. A., Vanualailai, J., Sharma, B., & Prasad, A. (2021). Velocity controllers for a swarm of unmanned aerial vehicles. *Journal of Industrial Information Integration*, *22*(1), 100198. https://doi.org/10.1016/j.jii.2020.100198

Matsikis, A., Schulte, F., Broicher, F., & Fraiss, K. F. (2003). A behaviour coordination manager for a mobile manipulator. In *Proceedings of the IEEE/RSJ International Conference on Intelligent Robots and Systems*, Las Vegas, USA (pp. 174–181).

Matychyn, I. (2020). Pursuit strategy of motion camouflage in dynamic games. *Dynamic Games and Applications*, *10*(1), 145–156. https://doi.org/10.1007/s13235-019-00316-0

Mehta, U., Alim, M., & Kumar, S. (2017). Smart path guidance mobile aid for visually disabled persons. *Procedia Computer Science*, *105*(5), 52–56. https://doi.org/10.1016/j.procs.2017.01.190

Padois, V., Fourquet, J.-Y., & Chiron, P. (2007). Kinematic and dynamic model-based control of wheeled mobile manipulators: a unified framework for reactive approaches. *Robotica*, *25*(2), 157–173. https://doi.org/10.1017/S0263574707003360

Pajak, G., & Pajak, I. (2017). Point-to-point collision-free trajectory planning for mobile manipulators. *Journal of Intelligent & Robotic Systems*, *85*(3–4), 523–538. https://doi.org/10.1007/s10846-016-0390-8

Papadopoulos, E., Papadimitriou, I., & Poulakakis, I. (2005). Polynomial-based obstacle avoidance techniques for nonholonomic mobile manipulator systems. *Robotics and Autonomous Systems*, *51*(4), 229–247. https://doi.org/10.1016/j.robot.2005.03.006

Papadopoulos, E., & Poulakakis, J. (2000). Planning and model-based control for mobile manipulators. In *Proceedings of the IROS Conference on Intelligent Robots and Systems*, Takamatsu, Japan.

Prasad, A., Sharma, B., & Vanualailai, J. (2014). A simple approach to motion control of a three-dimensional articulated manipulator arm. In *Asia-Pacific World Congress on Computer Science and Engineering* (pp. 1–7), Nadi, Fiji. IEEE.

Prasad, A., Sharma, B., & Vanualailai, J. (2017). A geometric approach to motion control of a standard tractor-trailer robot. In *2016 3rd Asia-Pacific World Congress on Computer Science and Engineering* (pp. 53–59), Nadi, Fiji. IEEE.

Raghuwaiya, K., Sharma, B., & Vanualailai, J. (2016). Cooperative control of multi-robot systems with a low-degree formation. In H. Sulaiman, M. Othman, M. Othman, Y. Rahim, & N. Pee (Eds.), *Advanced computer and communication engineering technology*. Lecture Notes in Electrical Engineering, Vol. 362 (pp. 233–249). Springer.

Raj, J., Raghuwaiya, K., & Vanualailai, J. (2020a). Collision avoidance of 3d rectangular planes by multiple cooperating autonomous agents. *Journal of Advanced Transportation*, 2020, 1–13. https://doi.org/10.1155/2020/4723687

Raj, J., Raghuwaiya, K., & Vanualailai, J. (2020b). Novel Lyapunov-based autonomous controllers for quadrotors. *IEEE Access*, *8*, 47393–47406. https://doi.org/10.1109/Access.6287639

Roennau, A., Heppner, G., Pfotzer, L., & Dillmann, R. (2013). Lauron V: Optimized leg configuration for the design of a bio-inspired walking robot. *Nature-Inspired Mobile Robotics*, 563–570. https://doi.org/10.1142/9789814525534_0071

Seraji, H. (1998). A unified approach to motion control of mobile manipulators. *International Journal of Robotics Research*, *17*(2), 107–118. https://doi.org/10.1177/027836499801700201

Sharma, B. N., Raj, J., & Vanualailai, J. (2018). Navigation of carlike robots in an extended dynamic environment with swarm avoidance. *International Journal of Robust and Nonlinear Control*, *28*(2), 678–698. https://doi.org/10.1002/rnc.v28.2

Sharma, B., Singh, S., Vanualailai, J., & Prasad, A. (2018). Globally rigid formation of n-link doubly nonholonomic mobile manipulators. *Robotics and Autonomous Systems*, *105*(3), 69–84. https://doi.org/10.1016/j.robot.2018.02.006

Sharma, B., Vanualailai, J., & Prasad, A. (2017). A $d\phi$-strategy: Facilitating dual-formation control of a virtually connected team. *Journal of Advanced Transportation*, *2017*, 1–17. https://doi.org/10.1155/2017/9213805

Sharma, B., Vanualailai, J., & Singh, S. (2012). Lyapunov-based nonlinear controllers for obstacle avoidance with a planar *n*-link doubly nonholonomic manipulator. *Robotics and Autonomous Systems*, *60*(12), 1484–1497. https://doi.org/10.1016/j.robot.2012.07.014

Sharma, B., Vanualailai, J., & Singh, S. (2015). Motion planning and posture control of multiple n-link doubly nonholonomic manipulators. *Robotica*, *35*(1), 1–25. https://doi.org/10.1017/S0263574714002604

Shojaei, K. (2015). Neural adaptive output feedback formation control of type (m, s) wheeled mobile robots. *International Journal of Adaptive*

Control and Signal Processing, *29*(7), 855–876. https://doi.org/10.1002/acs.v29.7

Tanner, H. G., & Kyriakopoulos, K. J. (2001). Mobile manipulator modeling with Kane's approach. *Robotica*, *19*(6), 675–690. https://doi.org/10.1017/S0263574701003381

Yamamoto, Y., & Yun, X. (1995). Coordinated obstacle avoidance of a mobile manipulator. In *Proceedings of the IEEE International Conference on Robotics and Automation* (Vol. 3, pp. 2255–2260), Nagoya, Japan. IEEE.

Appendix

We note that D_{ik}^* given in Section 5.2.2 is minimum if

$$\begin{aligned}
\gamma_{1k} = \min\{\max\{0, &(2a_{k3}(a_{k3}-b_{k3})+(a_{k1}-b_{k1})(a_{k1}-x_0)\\
&+(a_{k2}-b_{k2})(a_{k2}-y_0)+(b_{k1}-a_{k1})\ell_0\cos\vartheta\\
&+(a_{k1}^2+b_{k1}x_0-a_{k1}(b_{k1}+x_0)\\
&-(a_{k2}-b_{k2})(a_{k2}-y_0))\cos 2\vartheta\\
&+(b_{k2}-a_{k2})\ell_0\sin\vartheta-(-b_{k2}x_0+a_{k2}(b_{k1}+x_0)\\
&-b_{k1}y_0+a_{k1}(-2a_{k2}+b_{k2}+y_0))\sin 2\vartheta)\\
&/((a_{k1}+a_{k2}-b_{k1}-b_{k2})\\
&\times(a_{k1}-a_{k2}-b_{k1}+b_{k2})\cos 2\vartheta\\
&+2(a_{k1}-b_{k1})(a_{k2}-b_{k2})\sin 2\vartheta\\
&+(a_{k1}-b_{k1})^2+(a_{k2}-b_{k2})^2+2(a_{k3}-b_{k3})^2)\},1\},\\
\gamma_{2k} = \min\{\max\{0, &-((2a_{k3}(-a_{k3}+b_{k3})-(a_{k1}-b_{k1})(a_{k1}-x_0)\\
&-(a_{k2}-b_{k2})(a_{k2}-y_0)+(b_{k2}-a_{k2})w\cos\vartheta\\
&+(a_{k1}^2+b_{k1}x_0-a_{k1}(b_{k1}+x_0)\\
&-(a_{k2}-b_{k2})(a_{k2}-y_0))\cos 2\vartheta\\
&+(a_{k1}-b_{k1})w\sin\vartheta-(-b_{k2}x_0+a_{k2}(b_{k1}+x_0)-b_{k1}y_0\\
&+a_{k1}(-2a_{k2}+b_{k2}+y_0))\sin 2\vartheta)/(-(a_{k1}+a_{k2}-b_{k1}-b_{k2})\\
&\times(a_{k1}-a_{k2}-b_{k1}+b_{k2})\cos 2\vartheta\\
&-2(a_{k1}-b_{k1})(a_{k2}-b_{k2})\sin 2\vartheta)\\
&+(a_{k1}-b_{k1})^2+(a_{k2}-b_{k2})^2+2(a_{k3}-b_{k3})^2)\},1\},\\
\gamma_{ik} = \min\{\max\{0, &[((x_{i-1}-a_{k1})\cos\theta_i\cos(\theta_0+\vartheta)\\
&+(y_{i-1}-a_{k2})\cos\theta_i\sin(\theta_0+\vartheta)\\
&+(z_{i-1}-a_{k3})\sin\theta_i)((b_{k1}-a_{k1})\cos\theta_i\cos(\theta_0+\vartheta)\\
&+(b_{k2}-a_{k2})\cos\theta_i\sin(\theta_0+\vartheta)\\
&+(b_{k3}-a_{k3})\sin\theta_i)-((x_{i-1}-a_{k1})(b_{k1}-a_{k1})\\
&+(y_{i-1}-a_{k2})(b_{k2}-a_{k2})\\
&+(z_{i-1}-a_{k3})(b_{k3}-a_{k3}))]/[((b_{k1}-a_{k1})\cos(\theta_0+\vartheta)\\
&+(b_{k2}-a_{k2})\sin(\theta_0+\vartheta)\\
&+(b_{k3}-a_{k3})\sin\theta_i)^2\cos\theta_1-((b_{k1}-a_{k1})^2\\
&+(b_{k2}-a_{k2})^2+(b_{k3}-a_{k3})^2)]\},1\}
\end{aligned}$$

and

$$\begin{aligned}
\lambda_{0k}^* = \min\{\max\{0, &[a_{k3}((b_{k1}-a_{k1})^2+(b_{k2}-a_{k2})^2)\\
&+(b_{k3}-a_{k3})(-a_{k1}(b_{k1}-a_{k1})\\
&-a_{k2}(b_{k2}-a_{k2})+(b_{k1}-a_{k1})x_0\\
&+(b_{k2}-a_{k2})y_0)]/[a((b_{k1}-a_{k1})^2+(b_{k2}-a_{k2})^2)]\},1\},\\
\lambda_{1k}^* = \min\{\max\{&-\tfrac{1}{2},-((2w((-a_{k2}+b_{k2})\cos\vartheta\\
&+(a_{k1}-b_{k1})\sin\vartheta)(-2(a_{k3}(a_{k3}-b_{k3})\\
&+(a_{k1}-b_{k1})(a_{k1}-x_0)+(a_{k2}-b_{k2})(a_{k2}-y_0))\\
&+(a_{k1}-b_{k1})\ell_0\cos\vartheta+(a_{k2}-b_{k2})\ell_0\sin\vartheta)\\
&+4((a_{k1}-b_{k1})^2+(a_{k2}-b_{k2})^2\\
&+(a_{k3}-b_{k3})^2)w((-a_{k2}+y_0)\cos\vartheta+(a_{k1}-x_0)\sin\vartheta))\\
&/(-4((a_{k1}-b_{k1})^2+(a_{k2}-b_{k2})^2+(a_{k3}-b_{k3})^2)w^2\\
&+4w^2((a_{k2}-b_{k2})\cos\vartheta+(-a_{k1}+b_{k1})\sin\vartheta)^2))\},\tfrac{1}{2}\},\\
\lambda_{2k}^* = \min\{\max\{&-\tfrac{1}{2},-((2\ell_0((a_{k1}-b_{k1})\cos\vartheta\\
&+(a_{k2}-b_{k2})\sin\vartheta)(-2(a_{k3}(a_{k3}-b_{k3})\\
&+(a_{k1}-b_{k1})(a_{k1}-x_0)+(a_{k2}-b_{k2})(a_{k2}-y_0))\\
&+(-a_{k2}+b_{k2})w\cos\vartheta+(a_{k1}-b_{k1})w\sin\vartheta)\\
&+4((a_{k1}-b_{k1})^2+(a_{k2}-b_{k2})^2\\
&+(a_{k3}-b_{k3})^2)\ell_0((a_{k1}-x_0)\cos\vartheta+(a_{k2}-y_0)\sin\vartheta))\\
&/(-4((a_{k1}-b_{k1})^2+(a_{k2}-b_{k2})^2+(a_{k3}-b_{k3})^2)\ell_0^2\\
&+4((a_{k1}-b_{k1})\ell_0\cos\vartheta+(a_{k2}-b_{k2})\ell_0\sin\vartheta)^2))\},\tfrac{1}{2}\},\\
\lambda_{ik}^* = \min\{\max\{0, &[((a_{k1}-x_{i-1})(b_{k1}-a_{k1})\\
&+(a_{k2}-y_{i-1})(b_{k2}-a_{k2})+(a_{k3}-z_{i-1})(b_{k3}-a_{k3}))\\
&\times((b_{k1}-a_{k1})\cos\theta_i\cos(\theta_0+\vartheta)\\
&+(b_{k2}-a_{k2})\cos\theta_i\sin(\theta_0+\vartheta)+(b_{k3}-a_{k3})\sin\theta_i)\\
&-((b_{k1}-a_{k1})^2+(b_{k2}-a_{k2})^2\\
&+(b_{k3}-a_{k3})^2)((a_{k1}-x_{i-1})\cos\theta_i\cos(\theta_0+\vartheta)+(a_{k2}-y_{i-1})\\
&\times\cos\theta_i\sin(\theta_0+\vartheta)\\
&+(a_{k3}-z_{i-1})\sin\theta_i)]/[\ell_i((b_{k1}-a_{k1})\cos(\theta_0+\vartheta)\\
&+(b_{k2}-a_{k2})\sin(\theta_0+\vartheta)\\
&+(b_{k3}-a_{k3})\sin\theta_i)^2\cos\theta_1-\ell_i((b_{k1}-a_{k1})^2\\
&+(b_{k2}-a_{k2})^2+(b_{k3}-a_{k3})^2)]\},1\}.
\end{aligned}$$